POLITECNICO DI TORINO
Repository ISTITUZIONALE

Dynamic reduction technique for nonlinear analysis of spur gear pairs

(Article begins on next page)

14 October 2024

ORIGINAL PAPER

Dynamic reduction technique for nonlinear analysis of spur gear pairs

Fabio Bruzzone (ORCID) · **Carlo Rosso** (ORCID) · **Stephanos Theodossiades** (ORCID)

Abstract In this study the dynamic response of a spur gear pair is analyzed using a novel nonlinear approach. The actual rolling motion and engagement of the system is simulated using a set of reduced order models obtained in a pre-processing phase using the minimal amount of master degrees of freedom without loss of accuracy or generality. The flexibility of the gear bodies is included by a refined finite element model, and no geometry simplification is introduced while also retaining all nonlinearity sources. To reduce the computational cost the time-varying mesh stiffness is also pre-computed and used depending on the instantaneous loading conditions. Contact loss is also taken into account, and reconnection events are treated as vibro impacts. The results are compared against high quality and demanding experimental results with a computational cost several orders of magnitude lower than models with similar accuracy. Different loading conditions are investigated during the sweep-up and down maneuvers. Mainly, the dynamic transmission error is analyzed, showing remarkable agreement with the test campaign's results. Different nonlinear phenomena such as hysteretic jumps and sub- and super-harmonic resonances are correctly predicted by the proposed model in terms of both frequency and amplitude. This method allows quick and accurate nonlinear analyses overcoming current limitations and is open to further complications to include other components and effects.

Keywords Gears · Contact loss · TVMS · DTE

Fabio Bruzzone, Carlo Rosso and Stephanos Theodossiades have contributed equally to this work.

F. Bruzzone (✉) · C. Rosso
Department of Mechanical and Aerospace Engineering, Politecnico di Torino, Corso Duca degli Abruzzi 24, 10129 Turin, Italy
e-mail: fabio.bruzzone@polito.it

C. Rosso
e-mail: carlo.rosso@polito.it

F. Bruzzone · C. Rosso
GeDy TrAss s.r.l., Via Vela 42, 10128 Turin, Italy

S. Theodossiades
School of Mechanical, Electrical and Manufacturing Engineering, Loughborough University, Epinal Way, Loughborough, Leicestershire LE11 3TU, UK
e-mail: s.theodossiades@lboro.ac.uk

1 Introduction

The acceleration towards electric powertrains in response to environmental concerns has catalyzed a concerted effort within the automotive sector to confront the intricate challenges associated with the characteristics of noise, vibration, and harshness (NVH) of electric vehicles. A significant concern in this transition is the conspicuous absence of internal combustion engines, which, in turn, highlights the issue of pronounced gear vibrations during the meshing process. This phenomenon engenders the emergence of pervasive and often unwelcome gear whine noise. Evidently, the influence of these gear whine harmonics reaches beyond auditory discomfort, fundamentally

shaping the perceived sound quality of electric powertrains, making it a pivotal focal point within the field. In light of the pursuit to mitigate gear noise, considerable attention has been directed towards strategies that address the noise at its source, aiming for a more economically sustainable solution. In addition, the aviation industry is always seeking for increased performance and fuel efficiency, and lightweight gears are more and more employed to increase the power density of gearboxes. However, reducing the weight of those components leads to complex dynamic phenomena that need to be studied in detail to ensure the safety of the aircraft. Gear transmission systems have been widely studied, and deep understanding has been sought through a dual-pronged approach, encompassing both theoretical scrutiny and empirical investigation [1,2]. Parker and Vijayakar [3] presented an investigation into the dynamic response of a spur gear pair using a novel Finite Element (FE)/contact mechanics model. The study analyzes the behavior of the gear pair at various speeds and torques. One key feature of the model is that dynamic mesh forces are calculated using detailed contact analysis at each time step, eliminating the need for external specifications of excitation factors, although with a high computational cost. Contact loss of meshing teeth, even at high torques and with high-precision gears is investigated. The paper also explores the sensitivity of different models to the Fourier spectrum of changing mesh stiffness. The study underscores the importance of accurate dynamic modeling in understanding complex nonlinear behaviours in gear systems. Parker et al. [4] used the same formulation to analyze the dynamic response of a helicopter planetary gear system. The research uncovers resonances and interesting dynamics related to planetary configuration and mesh frequency harmonics. The torque sensitivity of the dynamic response is compared with static analyses, revealing different sensitivities between rotational and translational modes. Eritnel and Parker [5] presented an analytical solution for the nonlinear vibration of gear pairs with tooth surface modifications. The study introduces a force–deflection function obtained from independent sources, allowing the prediction of dynamic responses without predefined excitation or non-linearity. Also Benatar et al. [6] investigated the impact of tooth modifications on Static and Dynamic Transmission Error (STE, DTE) behaviour in helical gear pairs. The study uses a comprehensive experimental setup to quantify motion transmission

behaviour under varying torque and speed conditions, highlighting the influence of tooth modifications on the STE and DTE. Theodossiades and Natsiavas [7] investigated the nonlinear dynamics of a gear-pair system involving backlash and time-dependent mesh stiffness. The study identifies various types of periodic steady-state responses and their stability properties under specific forcing frequency ranges using strongly nonlinear equations of motion. The work sheds light on the complex resonant behaviour that arises due to simultaneous fundamental parametric resonance and external resonance conditions also found in planetary systems [8]. Natsiavas and Giagopoulos [9] focused on the systematic investigation of the response and stability characteristics of a gear pair system with strong non-linearities due to gear mesh backlash, static transmission error, and bearing clearance. The research uncovers a range of dynamic effects, including periodic, quasi-periodic, and chaotic motions, using analytical and numerical approaches. Natsiavas [10] surveys analytical modeling techniques for mechanical systems involving contact, impact, and friction. The study focuses on systems with a finite number of Degrees of Freedom (DoF) and examines various modeling approaches, including oscillators, deformable components, and techniques of nonsmooth mechanics. The review provides insights into modeling complex interactions in mechanical systems. Wang et al. [11] also explored chaos and bifurcation phenomena in a gear pair system with wear fault. A nonlinear time-varying dynamic model is used to analyze sub-harmonic and chaotic motions. However the cited works are not applicable in every scenario due to either their high computational cost or to simplifications in the geometry of the gear pair. Shweiki et al. [12] presented a hybrid FE-Analytical approach analyzing transmission error and strain in lightweight gear pairs. The method accurately captures gear deformation and strain distribution using a multibody solver. The approach is validated using experimental data from a gear test rig but is limited to static and quasi-static conditions. Palermo et al. [13] found a way to include the instantaneous contact conditions in a dynamic multibody model. Precomputed look-up tables are used to avoid cumbersome contact calculations at each time step with good results, but considering the gear bodies as rigid, limiting the applicability of their solution. Dai et al. [14] introduced a hybrid analytical-computational method to study the nonlinear dynamic response in spur gear pairs. The method

combines finite element static analysis with analytical vibration models, providing accurate predictions with significantly reduced computational time. The model captures complex behaviours, including partial contact loss and tooth modifications. The hybrid method developed exhibits high accuracy and efficiency compared to traditional finite element approaches. Its accuracy is, however, limited to cases in which the gear blank is stiff since the model assumes negligible gear blank vibrations. Pipitone et al. [15] focused instead on modeling the dynamics of thin-walled gears with time-varying coupling due to gear meshing. A nonlinear Method of Multiple-Time-Scales (MMTS) is utilized to analyze the coupled system. The MMTS approach demonstrates its capability to capture gear coupling effects and system dynamics, even in the presence of parametric variations such as mesh stiffness, without however introducing the possibility of contact loss and other non-linearities. Guilbert et al. [16] instead addressed the influence of centrifugal effects on thin-rim and webbed gears. An original hybrid gear model is introduced, incorporating lumped parameter elements to simulate gear behaviour. The model allows for the examination of gear whine simulation and highlights the impact of centrifugal effects on gear dynamics, but the starting gear model is simplified by removing the teeth, and no contact loss is possible.

The aim of this paper is to present a model capable of overcoming the limitations mentioned earlier. A novel approach to simulate the rolling motion and engagement of a gear pair using a Nonlinear Reduced Order Model (NL ROM) will be detailed. The simulation of the actual rotation and motion of the contact point using a ROM is not recorded in the literature to the knowledge of the authors. Implicit in the rolling motion is a nonlinear variation of the point of contact on the engaging teeth, which is further amplified by the Time-Varying Mesh Stiffness (TVMS). The TVMS will be precomputed using static analyses at different torque levels and will be used as a linear stiffness depending on the instantaneous dynamic loading conditions. Although in each time instant the model is linearised, the load dependency of the TVMS adds another degree of non-linearity to the system. Partial or total nonlinear contact loss will be introduced when traction forces are detected on the contact stiffness elements. After contact loss, the reconnection event will be treated as a Vibro Impact (VI) imposing a discontinuity of the velocities on the impacting flanks. Therefore, the
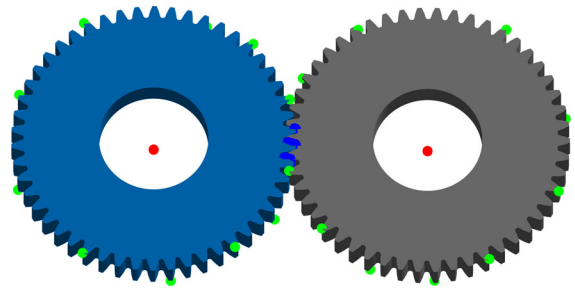

Fig. 1 Gear pair model with reduction nodes highlighted

proposed method globally takes into account several degrees of non-linearity. Another important aspect is that no geometrical simplification is needed for axially symmetrical gear bodies and their flexibility is taken in full account in dynamic conditions by the underlying FE model even though a minimal amount of master DoFs is selected. The resulting substantial reduction of the matrices' sizes opens the possibility for the simulation of long maneuvers in the time domain with an extremely limited computational cost without losing accuracy. The model has also a wide applicability since the reduction DoFs are independent on the number of teeth. The results of this model are compared with a high-quality campaign of experiments. The test gear pair exhibits distinct and repeatable nonlinear jump phenomena and parametric instabilities as well as sub- and super-harmonic resonances. Such complex nonlinear behaviour provides a highly demanding benchmark. The available DTE data exhibit remarkable agreement with the results of the model object of this study. Since both tooth and gear body geometry are fully represented, more complex analyses will be possible in the future using this approach for example on lightweight thin-webbed gear pairs.

2 Methodology

In this section the iterative algorithm to obtain the time domain response of a gear pair will be detailed. In order to achieve the desired result a pre-processing phase is needed. As stated in the introduction, the proposed method will employ a ROM to decrease the size of the matrices involved and hence reduce the otherwise impossibly long computational times. The meshing interaction of a gear pair is periodic in nature, and this can be exploited to obtain a ROM contain-

ing the minimum necessary DoFs to simulate the non-linear interaction and excitation typical of gears. If the body of the gears is axisymmetric, the geometrical properties of a gear are also cyclically symmetric. The period angle is $\theta = 360/Z_p$ where Z_p is the number of pinion teeth. Therefore, the properties of the FE model can also be considered periodic and in the proposed approach this cyclic repetition will enable selecting only a few nodes that fully represent one fundamental period of the dynamics of engagement. Gears rotate during engagement, and to simulate this motion a set of matrices, each rotated by an angle $\Delta\theta_p = \theta/N$, $\Delta\theta_g = -\tau\Delta\theta_p$, is first obtained for the pinion and gear, respectively, where N is the chosen number of subdivisions of the mesh cycle and τ is the transmission ratio. The FE stiffness and mass matrices ($K_{p,z}$, $M_{p,z}$, $K_{g,z}$, $M_{g,z}$) of the pinion (p) and gear (g) respectively are obtained using selective under-integration and an Enhanced Assumed Strain (EAS) field as described in [17] to avoid shear and volumetric locking as well as spurious modes in the 8 nodes hex-ahedral elements which comprise the entirety of the parametrically generated FE mesh. At the zth angular position ($z = 1, 2, \ldots, N$) the Craig-Bampton Component Mode Synthesis (CB-CMS) [18] is performed on each matrix to obtain the ROM matrices through the transformation matrices $T_{p,z}$ and $T_{g,z}$. The CB-CMS mass matrix of the assembled system at the zth angular position is obtained as

$$M_z^r = \begin{bmatrix} T_{p,z}^T & T_{g,z}^T \end{bmatrix} \begin{bmatrix} M_{p,z} & \mathbf{0} \\ \mathbf{0} & M_{g,z} \end{bmatrix} \begin{bmatrix} T_{p,z} \\ T_{g,z} \end{bmatrix} \quad (1)$$

and similarly for the system stiffness matrix

$$K_z^r = \begin{bmatrix} T_{p,z}^T & T_{g,z}^T \end{bmatrix} \begin{bmatrix} K_{p,z} & \mathbf{0} \\ \mathbf{0} & K_{g,z} \end{bmatrix} \begin{bmatrix} T_{p,z} \\ T_{g,z} \end{bmatrix} \quad (2)$$

where $\mathbf{0}$ is a zero matrix of suitable dimensions and the superscript r indicates that the matrix is reduced. The reduction basis is made of master nodes, where the forces will be exchanged and displacements recorded, and of auxiliary observed nodes, which help in increasing the accuracy of the ROM with respect to the full model mode shapes of interest for the frequency range chosen. Referring to Figs. 1 and 2, the different sets of nodes of the pinion and gear can be distinguished as follows:

- Contact mesh stiffness nodes $u_{Kc,p}$, $u_{Kc,g}$ (blue dots): The source of excitation of the whole system will be the periodic TVMS and the variation of the location of the contact stiffness connection points. This will be the main source of nonlinearities in the model.

- Auxiliary observed nodes $u_{aux,p}$, $u_{aux,g}$ (green dots): Those nodes are selected using a Modal-Geometrical Selection Criterion (MoGeSeC) [19] in order to select the nodes where the highest modal content is located to improve the accuracy of the ROM. These are not strictly master nodes, but they are only observed [17].

- Central virtual nodes $u_{t,p}$, $u_{t,g}$ (red dots): These nodes are master nodes of rigid joint connections linking the nodes on the inner radii of the pinion and the gear. The experimental test bench against which the results of the present model will be compared is designed to isolate the impact of tooth mesh. The configuration is such that the bearings and shafts are nearly rigid and the response is purely gear rotation. Hence, all DoFs of $u_{t,p}$, $u_{t,g}$ will be constrained, except for the rotational DoF around the axis of rotation for both pinion and driven gear which will be left unconstrained and here a constant torque will be applied on the pinion and an equal and opposing torque on the driven gear simulates the actual configuration of the test bench. Since both the pinion and gear hence have a free rigid body motion, their angular displacement of the centre node will be taken as the output DTE from the time domain response as

$$DTE(t) = \theta_p(t)r_{b,p} - \theta_g(t)r_{b,g} \quad (3)$$

where $\theta_p(t)$, $\theta_g(t)$ are the instantaneous angular displacements of said nodes for the pinion and gear respectively.

Extensive modal analyses have been performed to ensure the accuracy of the ROM. The pinion and gear have been analysed separately as well as coupled. Even though the CB-CMS is a fixed interface method, the auxiliary observed nodes provide an increment in accuracy and all simulations provided exceptional agreement between the full FE and ROM results. The frequencies of the first ten flexible modes of the uncoupled pinion, excluding the remaining rigid body mode, are listed in Table 1 and show a maximum percentage error
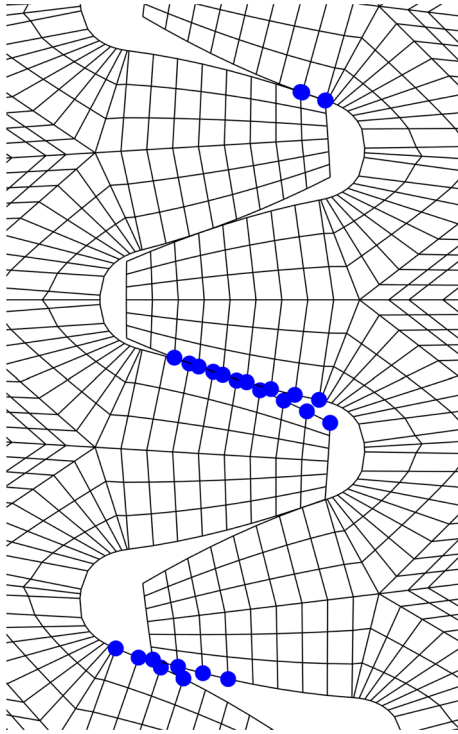
Fig. 2 Detail of the gear pair FE mesh and contact mesh stiffness nodes highlighted

Table 1 The first ten flexible modes of the pinion frequencies and percentage error between the full FE and ROM modal analysis

Mode N°	Frequency (Hz)	% error
1	7999.3	$-1 \cdot 10^{-5}$
2	7999.3	-0.02
3	8213.0	-0.01
4	8614.9	$-4 \cdot 10^{-4}$
5	8614.9	-0.03
6	11319.5	-0.01
7	11899.2	-0.02
8	11899.2	-0.05
9	17003.6	-0.01
10	17003.6	-0.01

of -0.05% with respect to the full FE results. Also the eigenvectors are coherent between each other as shown by the Modal Assurance Criterion (MAC [20]) visible in Fig. 3 which displays a minimum value of 88.9%.

The final vector of all considered DoFs in the analyses for the pinion and gear respectively are then
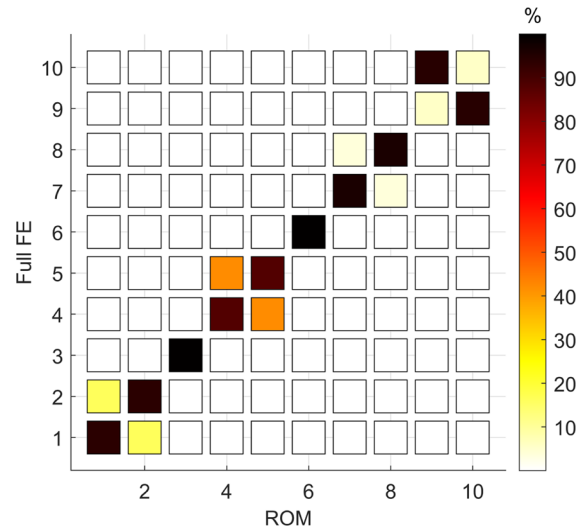
Fig. 3 MAC between the full FE and ROM modal analysis of the pinion

$$u_{m,p} = \{u_{t,p}^T u_{Kc,p}^T u_{aux,p}^T\}^T$$
$$u_{m,g} = \{u_{t,g}^T u_{Kc,g}^T u_{aux,g}^T\}^T \tag{4}$$

which is assembled as the system DoFs as

$$u_m = \{u_{m,p}^T u_{m,g}^T\}^T \tag{5}$$

The coupling between the pinion and the driven gear is realized by the time-varying, load dependent and moving mesh contact stiffness matrix $K_c(z, L)$. The individual elements of this matrix are linear springs connecting the relevant DoFs $u_{Kc,p}$ of the pinion to the corresponding $u_{Kc,g}$. The individual nodal matrix for a generic node n is

$$K_{c,n}(z, L) = w(z, L)_n \cdot k_c(z, L)$$
$$\cdot \begin{bmatrix} \cos\alpha & 0 & 0 \\ 0 & \sin\alpha \cdot \cos\beta & 0 \\ 0 & 0 & \cos\alpha \cdot \sin\beta \end{bmatrix} \tag{6}$$

where $w(z, L)_n$ is a weight factor for the nth node used to spread the stiffness across the facewidth of the gears and α and β are the pressure and helix angles of the gear pair. The individual nodal matrices are then assembled in the system contact stiffness matrix $K_c(z, L)$ with standard FE procedures [17]. At each time instant different DoFs will be connected simulating the motion of the contact across the height of the teeth. The value

of the TVMS $k_c(z, L)$ is obtained using the approach detailed in [21–23]. Since in the present model the flexibility of the tooth is included in the reduced FE matrices, only the contribution to the STE due to the contact stiffness STE_c is considered in its calculation as

$$k_c(z, L) = \frac{T(L)}{r_b \cdot STE_c(z)} \qquad (7)$$

where r_b is the base radius of the pinion and $T(L)$ is the torque applied at the Lth load level. In the direct time integration that will follow at each time step a different system matrix will be used, thus simulating the actual rotation of the gears involved. This implies that in the time integration the rotation covered between each time step will be $\Delta\theta_p$ and hence the interval Δt between two successive time instants will vary with speed. With the present approach any manoeuvre can be simulated but for the purpose of this article only constant variation will be detailed. Given a starting rotational velocity Ω_s and a final one Ω_f, the constant angular acceleration is simply obtained by

$$\dot{\Omega} = \frac{\Omega_f - \Omega_s}{t_{tot}} \qquad (8)$$

where t_{tot} is the total time in which the speed sweep will be simulated. The instantaneous rotational velocity Ω_i at a generic i^{th} time instant t_i is obtained by

$$\Omega_i = \Omega_{i-1} + \dot{\Omega} \cdot (t_i - t_{i-1}) \qquad (9)$$

where

$$t_i = t_{i-1} + \frac{-\Omega_{i-1} + \sqrt{\Omega_{i-1}^2 + 2\Delta\theta_p\dot{\Omega}}}{\dot{\Omega}} \qquad (10)$$

The dynamic response of the assembled system is obtained using a Newmark direct time integration scheme [24]. The constants used are

$$\alpha_{NM} = \frac{1}{4}, \delta_{NM} = \frac{1}{2} \qquad (11)$$

to enforce unconditional stability without introducing numerical damping. Regrouping the terms of the equation of motion to be solved the following equation is obtained for the ith timestep which corresponds to the zth angular position

$$\ddot{u}_i = S_i^{-1}\delta r_i \qquad (12)$$

where

$$S_i = M_{z,i}^r + \Delta t_i C_{z,i}^r + \Delta t_i^2 \alpha_{NM}(K_{z,i}^r + K_c^r(z, L)) \qquad (13)$$

and the Rayleigh reduced damping matrix is obtained as

$$C_z^r = [T_{p,z}^T\ T_{g,z}^T] \cdot \left(\mu\begin{bmatrix} K_{p,z} & 0 \\ 0 & K_{g,z} \end{bmatrix} + \eta\begin{bmatrix} M_{p,z} & 0 \\ 0 & M_{g,z} \end{bmatrix}\right)\begin{bmatrix} T_{p,z} \\ T_{g,z} \end{bmatrix} \qquad (14)$$

The residual vector δr_i is obtained from the following matrices

$$\begin{aligned} D_i &= -(K_{z,i}^r + K_c^r(z, L)) \\ V_i &= -C_{z,i}^r - \Delta t_i(K_{z,i}^r + K_c^r(z, L)) \\ A_i &= -C_{z,i}^r(1 - \delta_{NM})\Delta t_i \\ &\quad - (K_{z,i}^r + K_c^r(z, L))\left(\frac{1}{2} - \alpha_{NM}\right)\Delta t_i^2 \end{aligned} \qquad (15)$$

which are then assembled as

$$\delta r_i = f + D_i u_{i-1} + V_i \dot{u}_{i-1} + A_i \ddot{u}_{i-1} \qquad (16)$$

where $u_{i-1}, \dot{u}_{i-1}, \ddot{u}_{i-1}$ are respectively the displacements, velocities and accelerations of the system at the previous timestep. For the purpose of this article the external force vector f is constant throughout the entirety of the simulation and its only non null value will be the torque T applied to the free DoF at the center of the pinion. The acceleration at the current timestep is then computed as

$$\ddot{u}_i^* = S_i^{-1}\delta r_i \qquad (17)$$

and the velocities and displacements are obtained by

$$\begin{aligned} \dot{u}_i^* &= \dot{u}_{i-1} + (1 - \delta_{NM})\ddot{u}_{i-1} + \delta_{NM}\ddot{u}_i^*\Delta t_i \\ u_i^* &= u_{i-1} + \Delta t_i\dot{u}_{i-1} \\ &\quad + \Delta t_i^2\left(\frac{1}{2} - \alpha_{NM}\right)\ddot{u}_{i-1} + \alpha_{NM}\dot{u}_i^*\Delta t_i^2 \end{aligned} \qquad (18)$$

The displacements, velocities and accelerations u_i^*, $\dot{u}_i^*$, $\ddot{u}_i^*$ thus obtained are marked by the apex $*$ since they have been obtained using the zth set of matrices along the mesh cycle at timestep i, but for timestep $i+1$ the $(z+1)^{th}$ must be used. For this purpose a suitable rotation matrix $R_{\Delta\theta}$ of angles $\Delta\theta_p$ and $\Delta\theta_g$ is built using standard FE procedures [25] and applied to the current set of results to obtain a suitable set of inputs for the next timestep by

$$
\begin{aligned}
u_i &= R_{\Delta\theta} u_i^* \\
\dot{u}_i &= R_{\Delta\theta} \dot{u}_i^* \\
\ddot{u}_i &= R_{\Delta\theta} \ddot{u}_i^*
\end{aligned}
\tag{19}
$$

This iterative time advancement simulates the actual rotation of the gears in mesh and can continue until the end of the mesh cycle when $z = N$. Reaching that time condition, special measures have to be taken to reset the cycle to the initial geometrical conditions, while keeping the travelling wave of excitation continuous. Firstly the ROM results are expanded to obtain the full FE results using the transformation matrix $T_{cb,N}$ at the Nth angular position by

$$
\begin{aligned}
u_{i,F} &= T_{cb,N} u_i \\
\dot{u}_{i,F} &= T_{cb,N} \dot{u}_i \\
\ddot{u}_{i,F} &= T_{cb,N} \ddot{u}_i
\end{aligned}
\tag{20}
$$

where the subscript F indicates that they represent the full FE model of the assembled system and $T_{cb,N} = \begin{bmatrix} T_{p,N} \\ T_{g,N} \end{bmatrix}$. Pinion and gear displacement, velocities and accelerations are then separated and for a generic gear j ($j = p, g$) a sorting order can be found to group all the DoFs belonging to one tooth such that

$$
u_{j,F} = \left\{ \begin{array}{c} u_1 \\ u_2 \\ \vdots \\ u_{Z_j} \end{array} \right\}
\tag{21}
$$

A new sorting order advancing the generic gear of one tooth to start the new mesh cycle can then be imposed as

$$
u_{j,F'} = \left\{ \begin{array}{c} u_{Z_j} \\ u_1 \\ u_2 \\ \vdots \\ u_{Z_{j-1}} \end{array} \right\}
\tag{22}
$$

Selecting the same master DoFs described in Eq. 4 the new quantities for the next mesh cycle can finally be obtained as

$$
\begin{aligned}
u_i &= T_{r,1} R_{\Delta\theta} u_{i'} \\
\dot{u}_i &= T_{r,1} R_{\Delta\theta} \dot{u}_{i'} \\
\ddot{u}_i &= T_{r,1} R_{\Delta\theta} \ddot{u}_{i'}
\end{aligned}
\tag{23}
$$

where $T_{r,1} = \left(T_{cb,1}^T T_{cb,1} \right) T_{cb,1}^T$ is the system reduction matrix for $z = 1$ and $u_{i,F'}$, $\dot{u}_{i,F'}$, $\ddot{u}_{i,F'}$ are the displacements, velocities and accelerations in the newly sorted order.

A further non-linearity is introduced by considering the possibility of partial or total contact loss during the engagement dynamics. At each time instant the normal force exchanged by each contact stiffness element $F_{Kc,n}$ is monitored. If any traction force ($F_{Kc,n} < 0$) is detected the individual weight factor $w(z, L)_n$ for that element is set equal to 0 and the timestep is recomputed using the updated configuration up until an equilibrium is reached and all contact stiffness elements transmit null or compressive forces. The process is visualized in Fig. 4.

The normal separation $\delta_{Kc,mn}$ of a disconnected contact stiffness element connecting node m on the pinion ($u_{Kc,p,m}$) and n on gear ($u_{Kc,g,n}$) respectively is then monitored for the successive time instants. If $\delta_{Kc,mn} > 0$ the element is kept disconnected, while if $\delta_{Kc,mn} \leq 0$ the reconnection of the contact stiffness element is treated as a Vibro Impact (VI) [26]. Indicating with the superscripts $(-)$ and $(+)$ the velocities before and after the VI respectively a continuity of displacements and a discontinuity of velocities is imposed as

$$
\begin{aligned}
\dot{u}_{Kc,g,n}^{+} &= \frac{\dot{u}_{Kc,g,n}^{-}(1 - \epsilon \cdot e) + \epsilon \dot{u}_{Kc,p,n}^{-}(e+1)}{1+\epsilon} \\
\dot{u}_{Kc,p,n}^{+} &= \frac{\dot{u}_{Kc,g,n}^{-}(1 + e) + \epsilon \dot{u}_{Kc,p,n}^{-}(\epsilon - e)}{1+\epsilon}
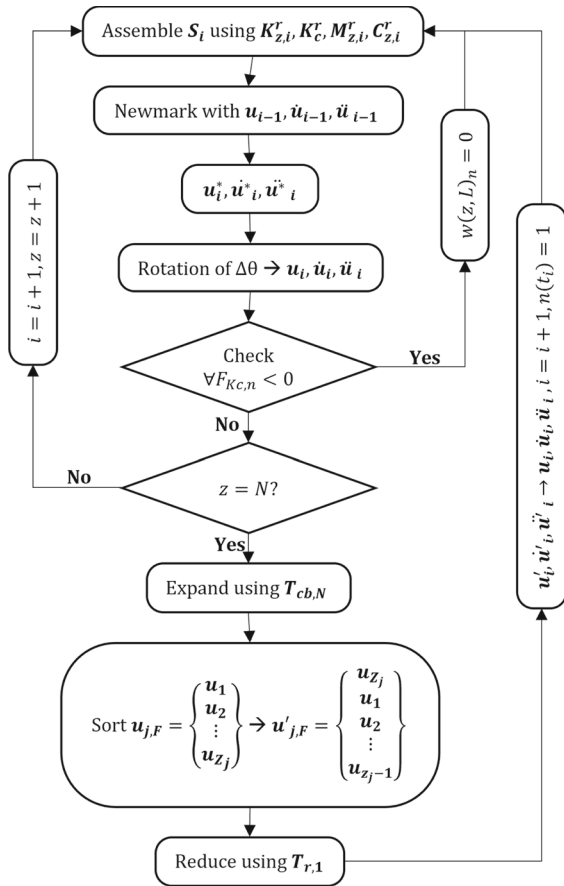\end{aligned}
\tag{24}
$$

Fig. 4 Algorithm of the NL ROM

Table 2 Pinion and gear geometrical and material data

Parameter	Value	Unit
Number of teeth, Z	50	–
Module, m	3	mm
Pressure angle, α	20	°
Facewidth, F	20	mm
Base radius, r_b	70.475	mm
Total backlash, $2B$	0.125	mm
Contact ratio	1.75	–
Modulus of elasticity, E	207	GPa
Density, ρ	7600	kg/m^3
Poisson ratio, ν	0.3	–
Coefficient of restitution, e	0.56	–
Full FE number of DoFs	270000	–
Pinion ROM number of DoFs	229	–
Gear ROM number of DoFs	229	–
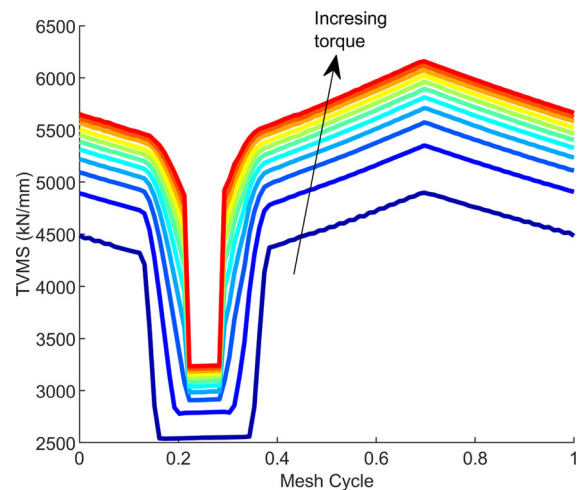
Fig. 5 TVMS map for torques from 10 to 500 Nm

where e is the coefficient of restitution and ϵ is the ratio of the equivalent masses of the pinion and the gear $\epsilon = \frac{I_g/r_{b,g}^2}{I_p/r_{b,p}^2}$ in which I_j and $r_{b,j}$ ($j = p, g$) are the moment of inertia and base radii of the respective gears.

3 Results

In order to validate the proposed model experimental data available in literature [27–29] are used for comparison. The main parameters of the steel precision ground spur gear pair are listed in Table 2. The TVMS map $k_c(z, L)$ computed using the semi-analytical approach detailed in [21–23] is visible in Fig. 5 for the range $10-500$ Nm and the Fourier spectrum for the first four harmonics is visible in Fig. 6 for a limited number of torque levels. The theoretical contact ratio of the gear pair is 1.75 but it evidently appears to be strongly influ-

enced by the applied load. Indeed, the single and double tooth contact zones greatly differ between low and high torque. This variation of the contact ratio with the applied load is also implicitly modeled in the proposed approach. In [27] it is stated that the torsional natural frequency of the gear pair system is around $\omega_n = 2700$ Hz. To estimate the torsional natural frequency of the model, impact tests were simulated numerically. The gear pair is kept in different fixed positions along the mesh cycle under constant torque except for a single time step in which the torque is increased of 40% on each side, simulating an impulse. The transient DTE
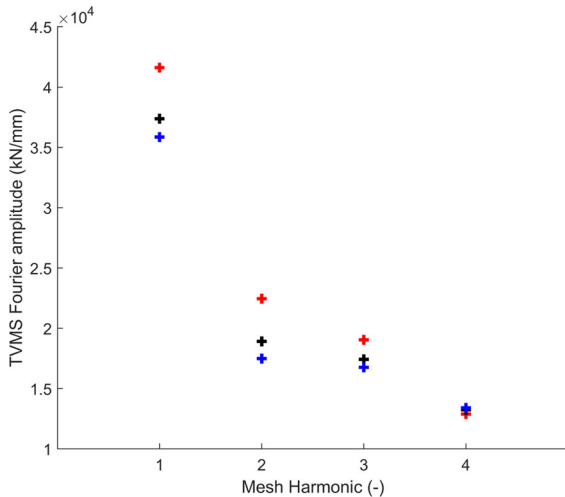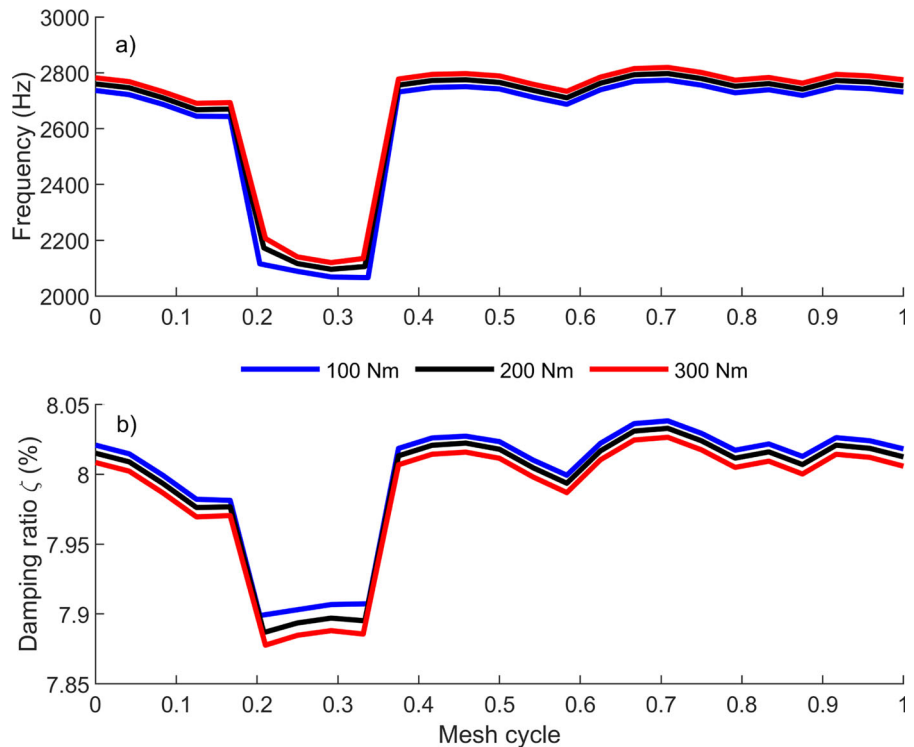
Fig. 6 TVMS Fourier spectrum for $T = 100$ Nm (blue), $T = 200$ Nm (black), $T = 300$ Nm (red)

response after the impulse is then used to determine the natural torsional frequency. Results are shown in Fig. 7-a and the obtained frequency is around 2650 Hz which is in excellent agreement with the experimental findings. The natural frequency appears to be a weak

function of the applied torque but is strongly affected by the contact state (single or double tooth contact).

The same numerical impact tests were used to set the coefficients μ and η of the structural damping model of Eq. 14. The logarithmic decrement [30] of the transient response was measured and the coefficients were adjusted to achieve a damping ratio close to 8% [31] as visible in Fig. 7b. Once set, the values have been kept constant for all the simulations. The main focus of this work is to study the dynamic response of the modeled system under different torques and at different rotational velocities. The nonlinear experimental DTE results for a torque $T = 150$ Nm are shown in Fig. 8 from [27]. The NL ROM results proposed in this paper are also compared in the same figure. The time domain simulations have been performed separately, slowly increasing and decreasing the rotational speed of the driving pinion in the 900–4100 RPM range corresponding to meshing frequencies in the range $f_m = 750$–3410 Hz. Both up and down sweeps simulated 25 s maneuvers with a calculation time of under 20 h in total without parallelization on a common desktop computer (Intel Core i7-11700K, 32 Gb RAM), excluding the preprocessing work, which can be done only once for a given gear pair. Each simulation comprises around 6

Fig. 7 Variation of the natural frequency (**a**) and damping ratio (**b**) of the system along the mesh cycle

Fig. 8 Experimental and NL ROM results of the RMS of the oscillating DTE component at $T = 150$ Nm
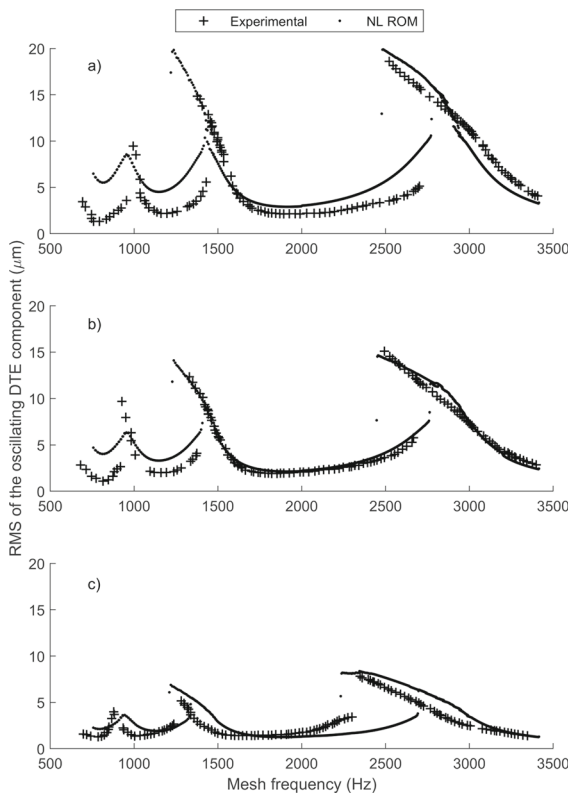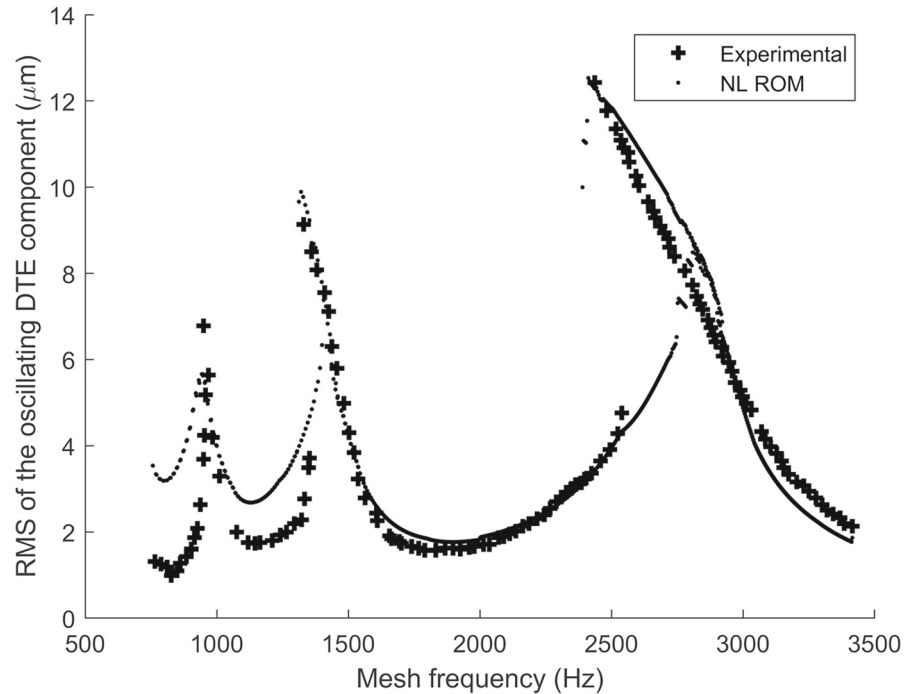

Fig. 9 Experimental and NL ROM results of the RMS of the oscillating DTE component at different torque levels: **a** $T = 300$ Nm, **b** $T = 200$ Nm, **c** $T = 100$ Nm

million timesteps. Considering that the solution time for each timestep is proportional to the square of the size of the matrices involved. Hence, several orders of magnitude of computational performance are gained with this approach as evident from Table 2 without any loss of accuracy with respect to full FE models.

A primary softening non-linearity peak is evident for mesh frequency $f_m \approx \omega_n \approx 2700$ Hz with multiple steady state solutions visible within the hysteretic jump region. Furthermore a second and third resonances are present. The second harmonic of the mesh frequency excites the resonance at $f_m \approx \omega_n/2 \approx 1350$ Hz while the third harmonics drives the one at $f_m \approx \omega_n/3$. The coexistence of multiple solutions, jump phenomena and branch softening are evident for the second harmonic but less pronounced for the third one.

All the distinctive features apparent from the experimental tests are accurately reproduced by the NL ROM model proposed in this work. The accuracy is evident both in terms of frequency but also in terms of amplitude of oscillation across the range of rotational velocity. Only the third super-harmonic appears to be underestimated by the numerical calculations, but the decreasing amplitude trend between the different resonances is respected. Figure 9 shows the experimental results for the torque levels $T = 100, 200$ and 300 Nm. Distinct multiple resonances and nonlinear phenomena

Fig. 10 DTE time histories and Fourier amplitudes for the **a**, **b** upper branch and **c**, **d** lower branch of the primary harmonic under $T = 150$ Nm at $f_m = 2400$ Hz
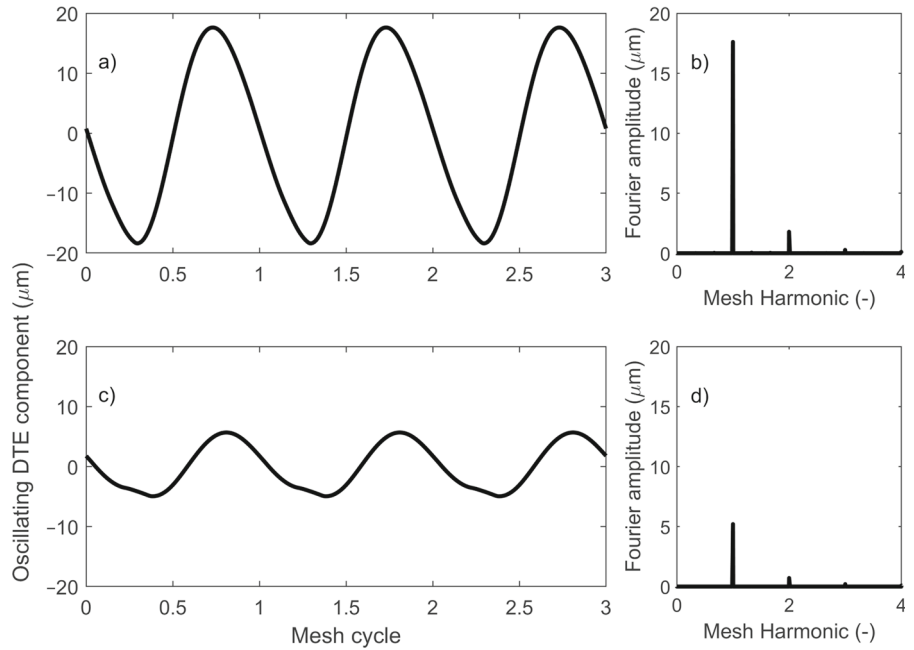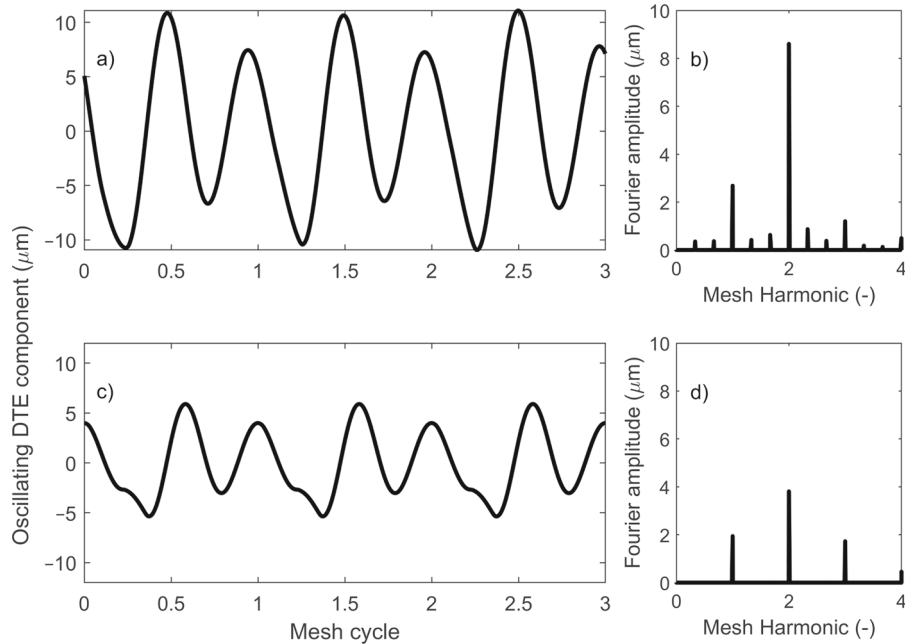
Fig. 11 DTE time histories and Fourier amplitudes for the **a**, **b** upper branch and **c**, **d** lower branch of the secondary harmonic under $T = 150$ Nm at $f_m = \omega_n/2 = 1350$ Hz

highlighted before are also evident in those results at both higher and lower torques. The corresponding simulation results of the NL ROM model are shown in the same graphs. Also in this case the responses show an excellent agreement against the experimental counterparts. The jump down frequency of the experimental results however shows a stronger variation with the applied torque which is less pronounced in the simulations. This is due to the fixed damping in the system which is kept constant for all torque levels and the absence of lubrication damping in the mesh process which will be included in future studies. However, the region of coexistence of multiple steady state solutions has a broader frequency overlap in the simulations with

Fig. 12 Tooth forces for the **a** upper branch and **b** lower branch of the primary harmonic under $T = 150$ Nm at $f_m = 2400$ Hz. Each line represents a different engaging tooth
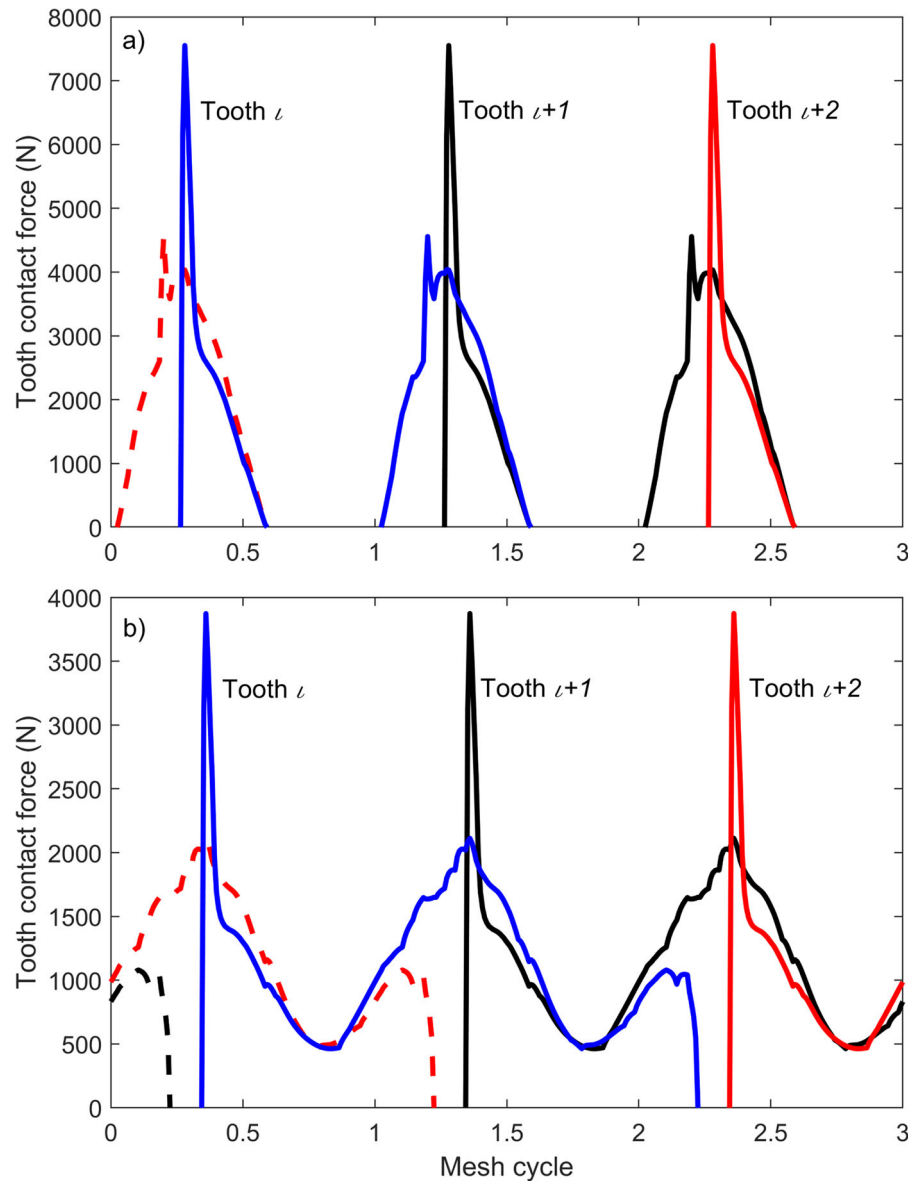
respect to the experimental findings. Figure 10 shows time domain results of the DTE and its spectral content in the region of primary resonance (multiple responses) for $T = 150$ Nm. The upper (Fig. 10a, b) and lower (Fig. 10c, d) branch results exhibit almost purely harmonic motion with limited contributions of the higher harmonics however with distinct vibration amplitudes between the two branches. For the second resonance condition similar results are visible in Fig. 11. Two oscillations are visible for each mesh cycle indicating that the response is almost harmonic at the mesh frequency which is in this case $f_m = \omega_n/2$. The upper

branch also shows traces of multiple harmonics also non integers of the mesh frequency due to the inclusion in the model of the flexible modes of the gear bodies while the lower branch shows harmonic content of the mesh frequency up to the fourth harmonic, still in excellent agreement with the results published in [27].

The softening behaviour of the system is explained by sustained total contact loss during meshing. In Fig. 12 the net tooth mesh force is visible for the upper and lower branches of the multiple solution region around $f_m = 2400$ Hz for $T = 150$ Nm. In the lower branch (b) of the primary resonance tooth loads are

Fig. 13 Tooth forces for the **a** upper branch and **b** lower branch of the primary harmonic under $T = 150$ Nm at $f_m = \omega_n/2 = 1350$ Hz. Each line represents a different engaging tooth
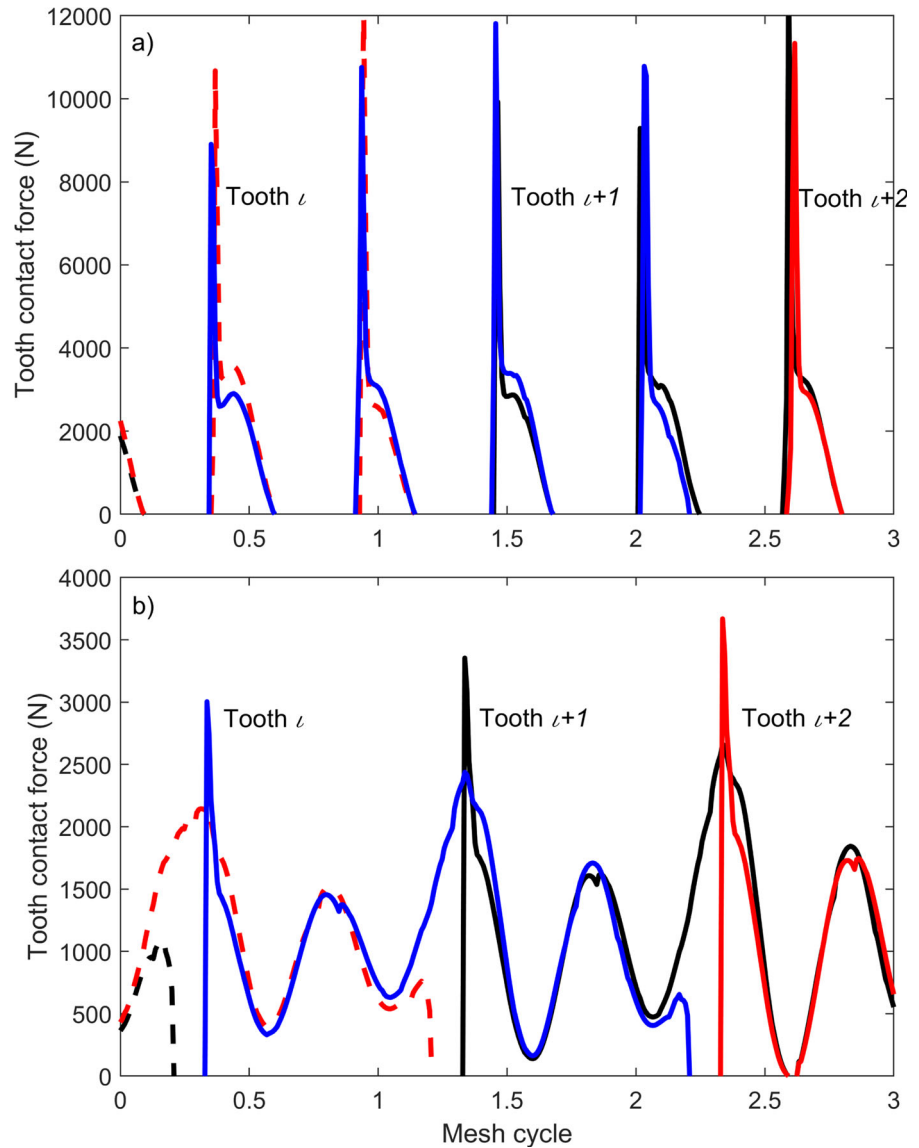
carried smoothly throughout the different mesh cycles, although a sharp force peak is evident in these conditions when the next available tooth comes into contact. This kind of event is not treated as a VI hence the force peak. In the upper resonance branch (a) however the forces vanish for almost half of the mesh cycle indicating total contact loss which is the clear source of the nonlinear multiple solution regime. Net forces are overall higher during the contact part of the mesh cycle and the impact when a tooth comes into contact is even more pronounced. Consistently, for $f_m = \omega_n/2 = 1350$ Hz two contact loss events are noticeable for each

mesh cycle as visible in Fig. 13a on the upper branch. Peak impact tooth loads are even higher in this scenario while on the lower branch load carrying is smooth and the force peaks are less pronounced.

4 Conclusions

This paper presents a novel methodology for fast and complex gear dynamic analyses. Using a reduced order approach all key nonlinear features of gear engagement are simulated. The cyclical variation of stiffness is simulated by the motion along the contacting

flanks of linearised stiffnesses. Those are precomputed and included in a TVMS map to avoid cumbersome contact calculations without any loss of accuracy or without introducing forced external excitation. In the present approach only the external forces are specified and are constant throughout each analysis presented but any load and speed variation can be simulated in the time domain. The nonlinear increase in the amplitude of vibration is indeed caused by the self excitation mechanism typical of gears and by contact loss in certain regimes of rotation and load. The rolling motion of the gears is completely included in the simulation using a very limited number of nodes. The transition from one mesh cycle to the next is smoothly carried out using an expansion, sorting and reduction strategy of the system's DoFs. This strategy minimizes the size of the matrices for the dynamic analyses allowing short calculations. Indeed several orders of magnitude of computational performance are gained by the proposed methodology making it competitive with analytical or semi-analytical methods. However, the geometry of the studied gears is precisely accounted for by the underlying FE model, without introducing any simplification. More complex geometries could be studied effortlessly, including thin rim designs. The results of this study are limited to the DTE in order to establish a solid foundation for future work and the excellent agreement with the experimental data available from literature demonstrates its ability to correctly capture complicated nonlinear phenomena but more comprehensive analyses can be carried out. The jump-up and jump-down phenomena were correctly captured as well as the amplitudes of oscillation and the occurrence of total contact loss. Computational times are fast and useful engineering insights can be obtained using the proposed approach when applied to industrial cases. Since it is based on FE, additional features can be easily introduced. The gear bodies can be naturally coupled with flexible shafts, and linear or nonlinear bearing models can be used to connect those to the gearbox housing if needed. Microgeometrical profile modifications can be easily included changing only the TVMS map without having to go through the preprocessing phase each time. Indeed, for the order of magnitude of those kind of modifications only the local contact stiffness changes, while the gear teeth are unaffected. Geometrical errors and tooth-to-tooth variability can also be accounted for in the same way. Since at all times the relative velocities of the contacting points are known, dynamic lubrication as well as surface roughness effects can also be included.

Data Availability Statement The contents of this paper are covered by patent Nº EP4016367A1 and partially included in "F. Bruzzone, 2D/3D Nonlinear and Non-Hertzian Tooth Deflection Analysis for Compliant Gear Dynamics, Ph.D Dissertation, Politecnico di Torino, 2020". The datasets generated and/or analysed during the current study are not publicly available due to the above patent, but are available from the corresponding author upon reasonable request.

Declarations

Conflict of interest The authors have no relevant financial or nonfinancial conflict of interest to disclose.

References

1. Ozguven, H.N., Houser, D.R.: Mathematical models used in gear dynamics—a review. J. Sound Vib. **121**(3), 383–411 (1988)

2. Bruzzone, F., Rosso, C.: Sources of excitation and models for cylindrical gear dynamics: a review. Machines (2020). https://doi.org/10.3390/machines8030037

3. Parker, R.G., Vijayakar, S.M., Imajo, T.: Non-linear dynamic response of a spur gear pair: modelling and experimental comparisons. J. Sound Vib. **237**(3), 435–455 (2000)

4. Parker, R.G., Agashe, V., Vijayakar, S.M.: Dynamic response of a planetary gear system using a finite ele-

ment/contact mechanics model. J. Mech. Des. **122**, 304–310 (2000)

5. Eritnel, T., Parker, R.G.: Nonlinear vibration of gears with tooth surface modifications. J. Vib. Acoust. **135**(051005), 1–11 (2013)

6. Benatar, M., Handschuh, M., Kahraman, A., Talbot, D.: Static and dynamic transmission error measurements of helical gear pairs with various tooth modifications. J. Mech. Des. **141**, 103301 (2019)

7. Theodossiades, S., Natsiavas, S.: Non-linear dynamics of gear-pair systems with periodic stiffness and backlash. J. Sound Vib. **229**(2), 287–310 (2000)

8. Mohammadpour, M., Theodossiades, S., Rahnejat, H.: Dynamics and efficiency of planetary gear sets for hybrid powertrains. Proc. Inst. Mech. Eng. C J. Mech. Eng. Sci. **230**(7–8), 1359–1368 (2016). https://doi.org/10.1177/0954406215590644

9. Natsiavas, S., Giagopoulos, D.: 25—non-linear dynamics of gear meshing and vibro-impact phenomenon pp. 773–792 (2010). https://doi.org/10.1533/9781845699932.2.773

10. Natsiavas, S.: Analytical modeling of discrete mechanical systems involving contact, impact, and friction. Appl. Mech. Rev. **71**(5), 050802 (2019). https://doi.org/10.1115/1.4044549

11. Wang, X.S., Wu, S.J., Hu, J.C., Chen, J.: Material Sciences and Manufacturing Technology, Advanced Materials Research, vol. 629, pp. 506–510. Trans Tech Publications Ltd (2013). https://doi.org/10.4028/www.scientific.net/AMR.629.506

12. Shweiki, S., Rezayat, A., Tamarozzi, T., Mundo, D.: Transmission error and strain analysis of lightweight gears by using a hybrid FE-analytical gear contact model. Mech. Syst. Signal Process. **123**, 573–590 (2019). https://doi.org/10.1016/j.ymssp.2019.01.024

13. Palermo, A., Mundo, D., Hadjit, R., Desmet, W.: Multibody element for spur and helical transmission error and the dynamic stress factor of spur gear pairs. Mech. Mach. Theory **62**, 13–30 (2013)

14. Dai, X., Cooley, C.G., Parker, R.G.: An efficient hybrid analytical-computational method for nonlinear vibration of spur gear pairs. J. Vib. Acoust. **141**(011006), 1–13 (2018)

15. Pipitone, E., Firrone, C.M., Zucca, S.: Application of multiple-scales method for the dynamic modelling of a gear coupling. Appl. Sci. (2019). https://doi.org/10.3390/app9061225

16. Guilbert, B., Velex, P., Cutuli, P.: Quasi-static and dynamic analyses of thin-webbed high-speed gears: centrifugal effect influence. Proc. Inst. Mech. Eng. C J. Mech. Eng. Sci. **233**(21–22), 7282–7291 (2019). https://doi.org/10.1177/0954406219855411

17. MacNeal, R.H.: Finite Elements: Their Design and Performance. Marcel Dekker (1993)

18. Craig, R.R., Bampton, M.C.C.: Coupling of substructures for dynamic analyses. AIAA J. **6**, 1313–1319 (1968)

19. Bonisoli, E., Delprete, C., Rosso, C.: Proposal of a modal-geometrical-based master nodes selection criterion in modal analysis. Mech. Syst. Signal Process. **23**, 606–620 (2009)

20. Allemang, R.J., Brown, D.L.: A correlation coefficient for modal vector analysis. In: Proceedings of the First IMAC, pp. 110–116 (1982)

21. Rosso, C., Bruzzone, F., Maggi, T., Marcellini, C.: A proposal for semi-analytical model of teeth contact with application to gear dynamics. In: 2019 JSAE/SAE Powertrains, Fuels and Lubricants (2019). https://doi.org/10.4271/2019-01-2269

22. Bruzzone, F., Maggi, T., Marcellini, C., Rosso, C.: 2D nonlinear and non-hertzian gear teeth deflection model for static transmission error calculation. Mech. Mach. Theory (2021). https://doi.org/10.1016/j.mechmachtheory.2021.104471

23. Bruzzone, F., Maggi, T., Marcellini, C., Rosso, C.: Gear teeth deflection model for spur gears: proposal of a 3d nonlinear and non-Hertzian approach. Machines (2021). https://doi.org/10.3390/machines9100223

24. Newmark, N.M.: A method of computation for structural dynamics. J .Eng. Mech. Div. **85**, 67–94 (1959)

25. MacNeal, R.H.: The Nastran Theoretical Manual. NASA (1976)

26. Karayannis, I., Vakakis, A.F., Georgiades, F.: Vibro-impact attachments as shock absorbers. Proc. Inst. Mech. Eng. C J. Mech. Eng. Sci. **222**(10), 1899–1908 (2008). https://doi.org/10.1243/09544062JMES864

27. Blankenship, G.W., Kahraman, A.: Gear dynamics experiments, part I: characterization of forced response. ASME Power Transmission and Gearing Conference, San Diego (1996)

28. Kahraman, A., Blankenship, G.W.: Gear dynamics experiments, part II: effect of involute contact ratio. ASME Power Transmission and Gearing Conference, San Diego (1996)

29. Kahraman, A., Blankenship, G.W.: Gear dynamics experiments, part III: effect of involute tip relief. ASME Power Transmission and Gearing Conference, San Diego (1996)

30. Inman, D.J.: Engineering Vibration. Prentice Hall (1996)

31. Guilbault, R., Lalonde, S., Thomas, M.: Nonlinear damping calculation in cylindrical gear dynamic modeling. J. Sound Vib. **331**(9), 2110–2128 (2012). https://doi.org/10.1016/j.jsv.2011.12.025